3 Biotech (2022) 12:162
https://doi.org/10.1007/s13205-022-03224-0

ORIGINAL ARTICLE

Molecular cloning, characterization, and in-silico analysis of L-asparaginase from Himalayan *Pseudomonas* sp. PCH44

Subhash Kumar[1,2] · Sanyukta Darnal[1,2] · Vijeta Patial[1,2] · Virender Kumar[1] · Vijay Kumar[1] · Sanjay Kumar[1] · Dharam Singh[1,2]

Received: 25 February 2022 / Accepted: 17 June 2022 / Published online: 9 July 2022

Abstract

L-Asparaginase (L-ASNase) is a key enzyme used to treat acute lymphoblastic leukemia, a childhood blood cancer. Here, we report on the characterization of a recombinant L-ASNase (*Ps*44-*asn* II) from *Pseudomonas* sp. PCH44. The gene was identified from its genome, cloned, and overexpressed in the host *Escherichia coli* (*E. coli*). The recombinant L-ASNase (*Ps*44-ASNase II) was purified with a monomer size of 37.0 kDa and a homotetrameric size of 148.0 kDa. The purified *Ps*44-ASNase II exhibited optimum activity of 40.84 U/mg in Tris–HCl buffer (50 mM, pH 8.5) at 45 °C for 15 min. It retained 76.53% of enzyme activity at 45 °C after 120 min of incubation. The half-life and K_d values were 600 min and 1.10×10^{-3} min^{-1}, respectively, at 45 °C. The kinetic constants values K_m and V_{max} were 0.56, 0.728 mM, and 29.41, 50.12 U/mg for L-asparagine and L-glutamine, respectively. However, k_{cat} for L-glutamine is more (30.91 s^{-1}) than L-asparagine (18.06 s^{-1}), suggesting that enzymes act more efficiently on L-glutamine than L-asparagine. The docking analysis of L-asparagine and L-glutamine with active site residues of the enzyme revealed a molecular basis for high L-glutaminase (L-GLNase) activity and provided insights into the role of key amino acid residues in the preferential enzymatic activities.

Keywords L-ASNase II · L-GLNase · Recombinant · Kinetics · In-silico · Docking

Introduction

L-Asparaginase (L-ASNase, EC 3.5.1.1) hydrolyses L-asparagine into aspartic acid and ammonia. The enzyme can deplete free L-asparagine from the bloodstream, hence finding its applications in treating acute lymphoblastic leukemia (ALL) (Kidd 1953; Hill et al. 1967; Silverman et al. 2001; Pui et al. 2009; Costa et al. 2022). Usually, blood cells can produce their L-asparagine due to L-asparagine synthetase activity, but cancerous blood cells cannot synthesize L-asparagine. Hence, L-ASNase treatment deprived cancerous blood cells of nutrition, leading to their apoptosis (Kelo et al. 2009; Soncini et al. 2020). Besides L-ASNase role in ALL, different strategies are underway to find a new role for L-ASNase as an anticancer medicine for lung and breast cancers (Baskar et al. 2018; Knott et al. 2018). It has application in the food industry to mitigate acrylamide formation in baked or fried foods (Kornbrust et al. 2009; Meghavarnam and Janakiraman 2018; Paul and Tiwary 2020). Additionally, L-ASNase-based biosensors have been designed to measure the concentration of free L-asparagine from the serum samples (Verma et al. 2007).

✉ Dharam Singh
dharamsingh@ihbt.res.in; dharams14@gmail.com

Subhash Kumar
subhashkumar136@gmail.com

Sanyukta Darnal
sanyukta2306@gmail.com

Vijeta Patial
vijetapatial16@gmail.com

Virender Kumar
virender1188@gmail.com

Vijay Kumar
vijay.hpu@gmail.com

Sanjay Kumar
sanjaykumar@ihbt.res.in

[1] Biotechnology Division, CSIR-Institute of Himalayan Bioresource Technology, Palampur, Himachal Pradesh 176 061, India

[2] Academy of Scientific and Innovative Research (AcSIR), Ghaziabad 201 002, India

L-ASNase is widely distributed in microbes, plants, and animals (Batool et al. 2016). However, microorganisms offer a convenient alternative for extracellular L-ASNase production and purification (Vimal and Kumar 2017; Tundisi et al. 2017). Microbes possess two different variants of L-ASNases based on their cellular localization with a variable affinity for L-asparagine. The cytoplasmic (type I) and periplasmic (type II) variants of L-ASNase have low and high specific activity for L-asparagine, respectively (Yun et al. 2007; Schalk et al. 2014). It has been suggested that the K_m value of L-ASNase must be in a lower micromolar range for efficient hydrolysis of ~50 µM blood L-asparagine concentration (Cooney et al. 1970). Currently, *E. coli* and *Erwinia chrysanthemi* (*E. chrysanthemi*) based commercial formulations of L-ASNase II are used in the chemotherapeutic treatment of ALL. However, the commercial formulations show hypersensitive and immunogenic responses during and after the treatment (Wang et al. 2009).

The evident limitations of currently used L-ASNase-based commercial drugs have shifted the researcher's focus on the periplasmic enzyme. The periplasmic enzymes are endotoxin-free and protease deficient, thus, helping in minimizing the side effects. Additionally, extracellular enzymes are promoted to proper folding by the suitable redox potential of periplasmic space (Singh et al. 2013; Wingfield 2015; Tundisi et al. 2017). Also, L-ASNase associated L-GLNase activity is thought to be partially responsible for the side effects (Batool et al. 2016; Hijiya and Van Der Sluis 2016). Therefore, overcoming the side effects of microbial L-ASNase treatment requires scientific interventions. The advances in biotechnology, and improved developmental plans for the existing products, bioprospecting for new and novel sources of the enzymes with lesser or no side effects are of prime importance for future L-ASNase-based drug commercialization.

Our lab has explored several bacteria from high-altitude regions for L-ASNase in the past few years (Kumar et al. 2019). Amongst, L-ASNase II of *Pseudomonas* sp. PCH44 (*Ps*44-ASNase II) has higher activity for L-glutamine than L-asparagine, reflecting the enzyme's specificity and uniqueness. The L-GLNase activity has also been reported from bacterial species such as *E. coli*, *Bacillus licheniformis*, *Rhizomucor miehei* (*R. miehei*), and *Erwinia carotovora* (*E. carotovora*) but to a lesser extent than L-ASNase activity (Narta et al. 2007; Mahajan et al. 2014; Huang et al. 2014; Labrou and Muharram 2016). The L-GLNase activity in L-ASNase II is considered a drawback for its applications in therapeutics. However, the presence of L-GLNase activity in *Ps*44-ASNase II is inevitable. Therefore, in the present study, we report whole-genome analysis, heterologous expression, biochemical, and in-silico characterization of the *Ps*44-ASNase II isolated from high-altitude niches of the Indian Himalayan region. Further, in-silico and comparative docking analysis of *Ps*44-ASNase II and *E. coli* L-ASNase (*Ec*-ASNase II) with L-asparagine and L-glutamine were carried out to understand the molecular basis for higher L-GLNase activity in *Ps*44-ASNase II.

Materials and methods

Materials and bacterial strains

NEB *Taq* DNA Polymerase, T4 DNA Ligase, FastDigest *Sac*II and *Xho*I endonuclease, 1.0 kb DNA ladder, HisPur Cobalt resin superflow were purchased from Thermo Fisher Scientific, USA. The expression vector pET-47b(+) and *E. coli* BL-21(DE3) were purchased from Novagen, USA. The amino acids (L-asparagine, L-glutamine), Nessler's reagent, inducer (IPTG, isopropy L-β-D-1 thiogalactopyranoside), and antibiotics such as kanamycin were obtained from Sigma-Aldrich, USA. All the media chemicals were obtained from HiMedia, India.

Bacterial isolate PCH44

The bacterial isolate PCH44 was previously isolated and identified in our laboratory (Thakur et al. 2018). It was screened qualitatively for L-ASNase activity on a modified M9 medium (components in g/L; 6.0 g $Na_2HPO_4.2H_2O$, 3.0 g KH_2PO_4, 0.5 g NaCl, 2.0 mM $MgSO_4.7H_2O$, and 0.1 mM $CaCl_2{\cdot}2H_2O$) supplemented with L-asparagine (0.5%, w/v) as a nitrogen source and glucose (0.2%, w/v) as a carbon source and phenol red (0.003%) as an indicator dye (Kumar et al. 2019). The plate was incubated at 28 °C up to 120 h, and a qualitative color change from yellow to pink was observed. PCH44 was cultured in a modified M9 medium, and quantitative L-ASNase activity was estimated from 12 to 35 h of incubation. The enzyme activity was checked after every 3 h interval using Nessler's method. The 16S rDNA-based molecular identification of strain PCH44 was carried out (3130 xl genetic analyzer, Applied Biosystems, USA). The EzTaxon server was used to examine the sequence obtained following 16S rDNA sequencing (http://www.eztaxon.org/), and a partial 16S rDNA sequence was submitted to GenBank database (Thakur et al. 2018; Kumar et al. 2019). The phylogenetic tree of 16S rDNA sequences was constructed using MEGA X (Kumar et al. 2018).

Whole-genome analysis of bacterial isolate PCH44

The genomic DNA of bacterial isolate PCH44 was isolated; DNA library preparation, and whole-genome sequencing were performed as described earlier (Kumar et al. 2020). Briefly, the quality and quantity of genomic DNA were estimated using a Dropsense96 (Trinean, Gentbrugge, Belgium)

and Qubit 2.0 Fluorometer (Invitrogen, USA) following the manufacturer's instructions. A PacBio RSII (Pacific Biosciences, Menlo Park, USA) was used to sequence the whole-genome. The sequenced data were assembled using Canu 2.1 (Koren et al. 2017). The genome sequence of *Pseudomonas* sp. PCH44 was deposited in GenBank under reference GCF_018304925.1 and the best matching genome was determined to be *Pseudomonas vlassakiae* (GCA_014269035.2) with an ANI similarity value of 96.28. The genome was annotated with the Prokaryotic Genome Annotation Pipeline (PGAP) (Tatusova et al. 2016) and the Rapid Annotation Subsystems Technology (RAST) (Aziz et al. 2008).

Bioinformatics analysis and cloning of the gene for L-ASNase

Gene encoding L-ASNase II was identified from the annotated genome and retrieved the sequence. The nucleotide sequence was analyzed and translated using the ExPASy translate tool (Swiss Institute of Bioinformatics). The molecular mass and theoretical isoelectric point (pI) of L-ASNase II were calculated using the ProtParam tool [https://web.expasy.org/protparam/]. SignalP 5.0 was used to ascertain the presence of signal peptide (Armenteros et al. 2019). The protein sequence was further analyzed in UniProt [https://www.uniprot.org/blast/] against the database sequence of L-ASNase. Multiple sequence alignment was performed using ClustalW [https://www.genome.jp/toolsbin/clustalw] and ESPript 3.0 (Robert and Gouet 2014).

The complete nucleotide sequence of *Ps*44-*asn* II (NCBI Protein ID: JIQ88_05230) was retrieved from the whole-genome of *Pseudomonas* sp. PCH44 (BioProject ID PRJNA689707). The forward (5′-TCCCCGCGGTTATGAAAGAAGCCGAAACCCAGCAG-3′) and reverse (5′-CCGCTCGAGTCAGTACTCCCAGAAAATCCGCTGCA-3′) primers for the *Ps*44-*asn* II gene flanked by *Sac*II and *Xho*I restriction sites (underlined), respectively, were designed excluding the signal peptide nucleotide sequences (75 bp). The properties (T_m, cross dimer, ΔG, and self-dimer) of designed primers were analyzed using NetPrimer (Premier Biosoft, USA). The genomic DNA (30–50 ng) of PCH44 was used to amplify *Ps*44-*asn* II. The PCR amplification was performed using initial denaturation for 3 min at 95 °C and 35 cycles of each of 30 s at 94 °C, 40 s at 53 °C, 1 min at 72 °C, and a final extension of 7 min at 72 °C. The amplified PCR product and the pET-47b(+) vector were double digested with *Sac*II and *Xho*I. The double-digested PCR product and plasmid were ligated using T4 DNA ligase. The standard heat-shock method was used to transform of the ligated product into the *E. coli* BL-21(DE3) (Bergmans et al. 1981) and further incubated overnight at 37 °C on LB plates containing antibiotic kanamycin (25.0 µg/mL). The positive clones carrying pET-47b-*Ps*44-*asn* II recombinant plasmid were confirmed by colony PCR and sequencing. The recombinant plasmid was extracted using a plasmid purification kit (Favorgen, Taiwan) and sequenced using a vector-specific primer (T7 P and T7 T). FinchTV 1.4 was used to analyze and get the consensus sequence.

Expression of *Ps*44-ASNase II in *E. coli* BL-21(DE3)

E. coli BL-21(DE3) culture harboruring recombinant pET-47b-*Ps*44-*asn* II plasmid was inoculated in 100.0 mL modified M9 medium supplemented with yeast extract (1.0%) and kanamycin (25.0 µg/mL), and kept for growth at 37 °C × 200 rpm. When the cell OD (600 nm) reached 0.8, the bacterial culture was induced by adding 0.5 mM IPTG to express *Ps*44-ASNase II. Bacterial culture was incubated for 16 h (overnight) at 37 °C. The cell pellet was recovered by centrifugation at 8000 *g* for 20 min, washed thoroughly with buffer (50.0 mM Tris–HCl, pH 8.5) to remove residual medium traces, and suspended in basic buffer (50.0 mM Tris–HCl: pH 8.5, 300.0 mM sodium chloride, and 5.0 mM imidazole). The cell suspension was sonicated (8 s pulse on; 10 s pulse off, and 30% amplitude) for 40 min on ice. The cell lysate was centrifuged at 8000 *g* for 25 min to obtain cell-free extract (CFE). The specific activity and total protein content of the CFE were also measured.

Purification of recombinant *Ps*44-ASNase II

*Ps*44-ASNase II was purified using affinity-based chromatography with HisPur Cobalt Superflow. The CFE (0.45 µM filtered) was loaded onto the HisPur Cobalt Superflow chromatography column pre-equilibrated with a basic buffer. The matrix was washed with 10 column volumes (CV) of basic buffer to remove non-specific proteins. The bound *Ps*44-ASNase II was eluted using elution buffer (50.0 mM Tris–HCl pH 8.5, 300.0 mM NaCl, and 150.0 mM imidazole) in different fractions. The amount of protein in each fraction was estimated by Bradford assay (Bradford 1976) using bovine serum albumin as standard. The purity of different fractions was analyzed by 10% SDS-PAGE (Laemmli 1970). The purified fractions were pooled and dialyzed using 50.0 mM Tris–HCl (pH 8.5). The native molecular weight of purified *Ps*44-ASNase II was determined by gel exclusion chromatography (Superdex 200, GE Healthcare, USA) using different molecular weight markers (Merck-Sigma Aldrich, USA).

*Ps*44-ASNase II assay

The activity of *Ps*44-ASNase II was estimated spectrophotometrically (Synergy H1, BioTek, Agilent, USA) at 480 nm using Nessler's reagent, which measures the amount of

ammonia released in the reaction mixture (Imada et al. 1973). Briefly, the enzyme assay was performed in a 1.0 mL volume of a reaction containing 50.0 mM Tris–HCl, 5.0 mM L-asparagine, and 2.0 µg (enzyme suspension in reaction buffer) of purified *Ps*44-ASNase II. All reaction components were pre-incubated at 37 °C for 30 min. The reaction was carried out at 37 °C for 15 min and terminated by adding 250.0 µL (1.5 M) of TCA (Trichloroacetic acid). The control and blank were prepared simultaneously. The reaction was diluted as per necessity before adding Nessler's reagent, and the optical density was measured at 480 nm. A standard curve was also prepared using ammonium chloride. The specific activity of purified *Ps*44-ASNase II was expressed in U/mg protein (µmoles min^{-1} mg^{-1}). One unit (IU) of *Ps*44-ASNase II is defined as the amount of enzyme liberating 1.0 µmol of ammonia per minute under standard reaction conditions.

Biochemical characterization and kinetic evaluation of *Ps*44-ASNase II

The biochemical parameters for maximum *Ps*44-ASNase II activity were assessed. *P*s44-ASNase II activity was measured in 50.0 mM buffer of sodium citrate (pH 3.0–5.0), potassium phosphate (pH 6.0–7.0), Tris–HCl (pH 8.0–10.0), sodium carbonate-bicarbonate (pH 9.0–10.0), sodium carbonate-NaOH (pH 10.0–11.0), and potassium chloride-NaOH (pH 11.0–13.0). The buffer system with maximum activity was selected for further experiments. The ambient temperature of *P*s44-ASNase II was optimized by assaying the enzyme activity at different temperatures range (10–80 °C). The thermal stability of purified *P*s44-ASNase II was investigated. The enzyme was incubated at 28, 37, 45, 50, and 60 °C in 50.0 mM Tris–HCl buffer (pH 8.5), and residual enzyme activity was measured at fixed time intervals. The half-life of *P*s44-ASNase II was calculated from the thermal stability graph. Similarly, the specificity of *Ps*44-ASNase II for L-asparagine and L-glutamine was measured at different concentrations (0.05–5.0 mM). The K_m and V_{max} were calculated using the Michaelis–Menten equation and plotting 1/*s* and 1/*v* values in the Lineweaver–Burk plot. The k_{cat} of the *P*s44-ASNase II was deduced by using the equation $k_{cat} = V_{max}/[E_0]$, where $[E_0]$ is the initial enzyme concentration in the reaction and V_{max} (µmol/min) is the maximum reaction rate.

Effect of metal ions and protein modifying agents

The effect of various metal ions and protein modifying agents on purified *Ps*44-ASNase II activity was examined. The *Ps*44-ASNase II was pre-incubated at 37 °C for 60 min with 1.0 mM $CuSO_4$, $CoCl_2$, and 2.0 mM KCl_2, NaCl, $CaCl_2$, and $ZnSO_4$ in separate reactions. Similarly, the effect of protein-modifying agents using 1.0 mM dithiothreitol (DTT), sodium dodecyl sulfate (SDS), and 2.0 mM dimethyl sulfoxide (DMSO), ethylenediaminetetraacetic acid (EDTA), phenylmethylsulfonyl fluoride (PMSF), and 2-mercaptoethanol (β-ME) were also measured.

Homology modeling and structural validation of *Ps*44-ASNase II

A template search for homology modeling of *Ps*44-ASNase II was performed using BLASTp (http://blast.ncbi.nlm.nih.gov/) against the Protein Data Bank (PDB). The homology model of *Ps*44-ASNase II was generated using SWISS-MODEL v.4.0 (https://swissmodel.expasy.org/) based on predicted PDB structure with maximum sequence identity and percent coverage (Arnold et al. 2006). The quality of the model was assessed by analyzing the Ramachandran plot, PROCHECK, and structural analysis and verification server (SAVES v5.0) (https://saves.mbi.ucla.edu/). The secondary structure was predicted using SOPMA (Geourjon and Deleage 1995).

Docking analysis of *Ps*44-ASNase II and *Ec*-ASNase II

Three-dimensional structures of L-asparagine and L-glutamine were used as ligands for docking and were downloaded from the library of 3D Molecular Structures (https://pubchem.ncbi.nlm.nih.gov/compound/). The ligands were docked with the catalytic site of *Ps*44-ASNase II (Thr21 and Thr101) and *Ec*-ASNase II (Thr12 and Thr89) using Auto Dock Vina software (Trott and Olson 2010). The docked complexes of *Ps*44-ASNase II were evaluated for the amino acid-ligand interactions in close proximity (≤3 Å) of a catalytic site using Molegro Molecular viewer and LIGPLOT$^+$ (Laskowski and Swindells 2011). Further, a comparative analysis of the interactions of L-glutamine with catalytic sites of *Ps*44-ASNase II is performed with that of *Ec*-ASNase II to address the molecular basis of high L-GLNase activity in *Ps*44-ASNase II.

Statistical analysis

All the experiments were performed in triplicates. The data were represented in the form of mean ± standard deviation (±SD).

Results and discussion

Screening of PCH44 for L-ASNase activity

In our earlier studies, the bacterial isolate PCH44 was qualitatively screened for L-ASNase activity on a modified M9

medium (Kumar et al. 2019). The formation of pink color was observed after 48 h for every 24 h interval, suggesting L-ASNase producing ability (Fig. S1). Quantitatively, L-ASNase activity was measured after 12 h and subsequent readings after every 3 h intervals. The maximum enzymatic activity (0.58 U/mL crude) was obtained after 15 h of incubation at 28 °C and 180 rpm. Interestingly, the isolate PCH44 produces high L-ASNase-associated L-GLNase activity in a short time (15 h) compared to other potential isolates studied earlier (Kumar et al. 2019). Therefore, the PCH44 was selected for whole-genome sequencing to reveal genomic insights. The phylogenetic tree of 16S rDNA sequencing of isolate PCH44 (GenBank accession number KY628862) showed the best match with *Pseudomonas alloputida* Kh7(T) (Fig. S2) (the earlier best match was with *Pseudomonas hunanensis*) (Thakur et al. 2018).

Whole-genome analysis and in-silico characterization

The PacBio RSII platform was used to sequence the whole-genome of *Pseudomonas* sp. PCH44. The raw sequences were assembled using Canu 2.1 and generated seven contigs with a total genome size of 6.41 Mb. The genome was submitted to the NCBI database under the BioProject ID PRJNA689707 and BioSample ID SAMN17215112. The RAST server displayed 536 subsystems, 6092 coding sequences, and 62.2% GC content (Fig. S3 and Table S1). The two L-ASNase protein sequences (NCBI Protein ID: JIQ88_05230 and JIQ88_19890) were identified through PGAP and RAST annotation server. SignalP 5.0 server revealed the presence of signal peptide in JIQ88_05230 only, which corresponds to periplasmic localization. The pI of periplasmic *Ps*44-ASNase II was calculated at 6.33 using the ProtParam tool (Table S2). The periplasmic L-ASNase protein-encoding gene with signal peptide was selected for heterologous expression.

Cloning, expression, and purification of *Ps*44-ASNase II

The L-*asn* II gene (1.0 kb) was amplified using gene-specific primers (Fig. S4). The L-*asn* II was cloned and expressed in the host *E. coli* BL-21(DE3) under the control of T7 promoter in pET-47b(+) vector. The positive clones were grown in a modified M9 media and induced with 0.5 mM IPTG to express a heterologous protein. Maximum expression of *Ps*44-ASNase II was obtained at 37 °C after 20 h incubation. After expression, cell pellet was lysed, and *Ps*44-ASNase II was obtained as soluble and active CFE. The CFE was subjected to purification using HisPur Cobalt Superflow Agarose. The purified *Ps*44-ASNase II was obtained from CFE in a single chromatographic step. A final yield of 55.88% with 28-fold purification was achieved (Table 1). *Ps*44-ASNase II was obtained as a single distinct band of 37.0 kDa on SDS-PAGE analysis (Fig. 1A). The native molecular weight was estimated at 148.0 kDa, revealing a tetrameric form of *Ps*44-ASNase II, consistent with earlier reported native protein size (Fig. 1B). It was similar in size to L-ASNase of *E. coli*, used to treat ALL (Jackson and Handschumacher 1970). Also, L-ASNase from *E. carotovora* and *Vibrio cholerae* (*V. cholerae*) has a molecular weight of 36.6 kDa (Warangkar and Khobragade 2010; Radha et al. 2018), suggesting the expected size of *Ps*44-ASNase II.

Effect of pH on *Ps*44-ASNase II activity

The buffering environment of the reaction is a key deciding factor for optimal enzyme activity. In the present study, maximum *Ps*44-ASNase II activity (34.48 ± 3.79 U/mg) was observed in 50.0 mM Tris–HCl buffer (pH 8.5). The comparable activity (26.83 ± 2.39 U/mg) was also reported in potassium phosphate buffer (pH 7.5). However, Tris–HCl provides optimum buffering conditions with enhanced stability (Fig. S5). *Ps*44-ASNase II was found active in a broad pH range from 4.5 to 11.0 (Fig. 2A). In a similar study, L-ASNase from *Bacillus* sp. was reported to be active over a pH range between 4.5 and 10.0 (Safary et al. 2019). Also, the optimum pH of 8.5 for L-ASNase in the current study was similar to earlier reported pH from *Yersinia pseudotuberculosis* (*Y. pseudotuberculosis*, pH 8.0), *Staphylococcus* sp. OJ82 (pH 8.0–9.0), and *Halomonas elongate* (*H. elongate*, pH 8.0) (Pokrovskaya et al. 2012; Han et al. 2014; Ghasemi et al. 2017). The optimum enzyme activity of pH 8.0 is critical for therapeutic application since blood pH ranges from 7.35 to 7.45.

Table 1 Protein purification profile of recombinant *Ps*44-ASNase II expressed in *E. coli* BL-21(DE3) by HisPur Cobalt Superflow affinity chromatography

	Volume (mL)	Total protein (mg)	Specific activity (U/mg)	Total activity (U)	Purification fold	Yield (%)
Crude	24.0	77.76	1.0	77.76	1.0	100.0
His-Tag Affinity	3.0	1.55	28.0	43.45	28.0	55.88

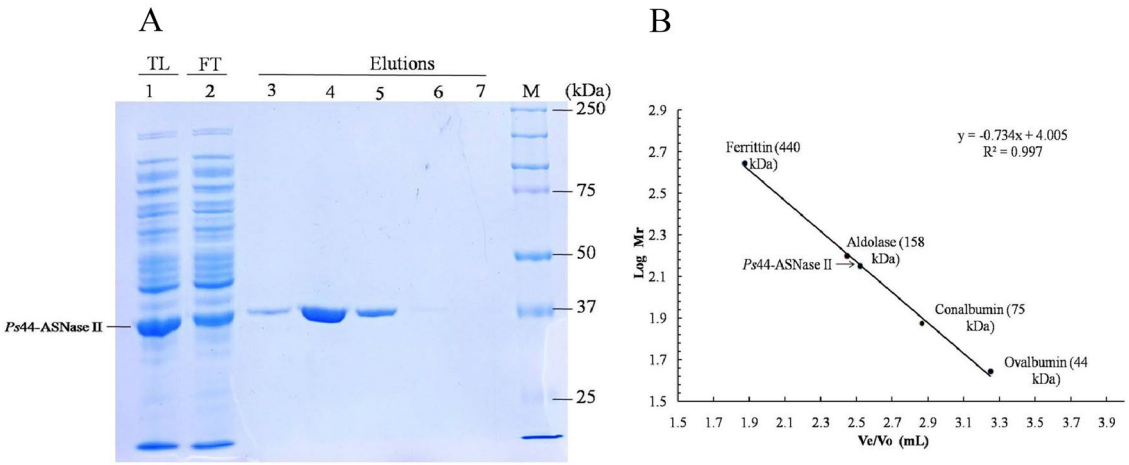

Fig. 1 Polyacrylamide gel electrophoresis and molecular weight estimation of *Ps*44-ASNase II. **A** SDS-PAGE (10%) analysis of recombinant *Ps*44-ASNase II. Lane 1 is total cell lysate; lane 2 is flow-through; lane 3–6 eluted protein; lane 7 is a wash, and M is protein molecular weight marker. **B** Determination of the molecular mass of the native *Ps*44-ASNase II. Gel filtration chromatography was performed using Superdex 200 (10/300 GL) column. Arrow indicates the log MW of the *Ps*44-ASNase II. Ferritin, aldolase, conalbumin, and ovalbumin were used as protein molecular weight standards for standard curves. V_e and V_o indicate for elution volume of each protein and void volume, respectively

Effect of temperature on *Ps*44-ASNase II activity

The purified *Ps*44-ASNase II exhibited activity at a temperature range from 10 to 75 °C with optimum activity at 45 °C (40.84 ± 0.9 U/mg). Above 50 °C, a sharp decrease in specific activity was observed (Fig. 2B). In literature, purified L-ASNase from *E. chrysanthemi* NCPPB1125 and *Paenibacillus barengoltzii* (*P. barengoltzii*) has optimum activity at 45 °C (Nguyen et al. 2016a, b; Shi et al. 2017). L-ASNase of *Pyrococcus furiosus* (*P. furiosus*) showed optimum activity at 50 °C (Saeed et al. 2020). The thermostability of *Ps*44-ASNase II was evaluated by incubating enzyme at different temperatures. *Ps*44-ASNase II retained 76.53% of enzyme activity at 45 °C after 120 min of incubation (Fig. 2C). The thermal inactivation of *Ps*44-ASNase II follows the theoretical curve of a first-order reaction. The half-life ($t_{1/2}$) of *Ps*44-ASNase II was calculated using linear regression of data acquired from thermal stability. The $t_{1/2}$ of *Ps*44-ASNase II at 45 °C in Tris–HCl (pH 8.5) was 600 min with a dissociation constant (K_d) of 1.10×10^{-3} min^{-1} (Table S3). L-ASNase from *P. furiosus* showed 72% residual activity after 60 min at 45 °C (Saeed et al. 2020). The $t_{1/2}$ (min) values for *V. cholerae* at 40 and 45 °C were 751 ± 21.5 and 13.6 ± 0.38, and the K_d (min^{-1}) values were 0.92×10^{-3} and 51.2×10^{-3} at 40 and 45 °C, respectively (Radha et al. 2018).

Effect of metal ions and protein modifier agents

Enzyme was assayed in the presence of different metal ions and protein modifying agents. It was found that none of the metal ions have a positive effect on *Ps*44-ASNase II activity (Fig. 2D). The presence of Ca^{2+}, K^+, Na^+, Zn^{2+}, Co^{2+}, and Cu^{2+} ions in reaction decreases the enzymatic activity. The high inhibitory effect of Zn^{2+} (52%) and EDTA (36%) on *Ps*44-ASNase II activity was reported. Inhibition of enzyme activity by using divalent ions might be due to the chelation of sulfhydryl groups of enzyme with metal ions. The sulfhydryl groups are critically important for enzyme activity to produce catalysis (Sokolov 1976; Radha et al. 2018). It showed that the *Ps*44-ASNase II does not essentially require monovalent and divalent ions for its activity. Besides DTT, protein modifiers like PMSF, β-ME, SDS, and DMSO had negatively affected the enzyme activity (Fig. 2D). The inhibition of L-ASNase activity by metal ions such as Zn^{2+} in *V. cholerae* (Radha et al. 2018), Cu^{2+}, Ca^{2+}, and Zn^{2+} in *P. furiosus* (Saeed et al. 2020) has also been reported. The Cu^{2+} showed inhibition in *Streptomyces brollosae* NEAE-115 (*S. brollosae*) L-ASNase (El-Naggar et al. 2018) and a complete loss of enzyme activity in *V. cholerae* L-ASNase (Radha et al. 2018) was observed. Similarly, protein-modifying agents such as SDS, EDTA, and β-ME also had an inhibitory effect on L-ASNase activity of *R. miehei* (Huang et al. 2014). DTT is widely used for protein structure maintenance by establishing a reducing environment for the SH group of cysteine-containing proteins. For instance, 1.0 mM DTT enhanced the activity of *E. coli* L-ASNase by 46% (Nguyen et al. 2016a, b). However, cysteine residue was not found in *Ps*44-ASNase II in this investigation. As a result, the addition of DTT did not affect enzyme activity.

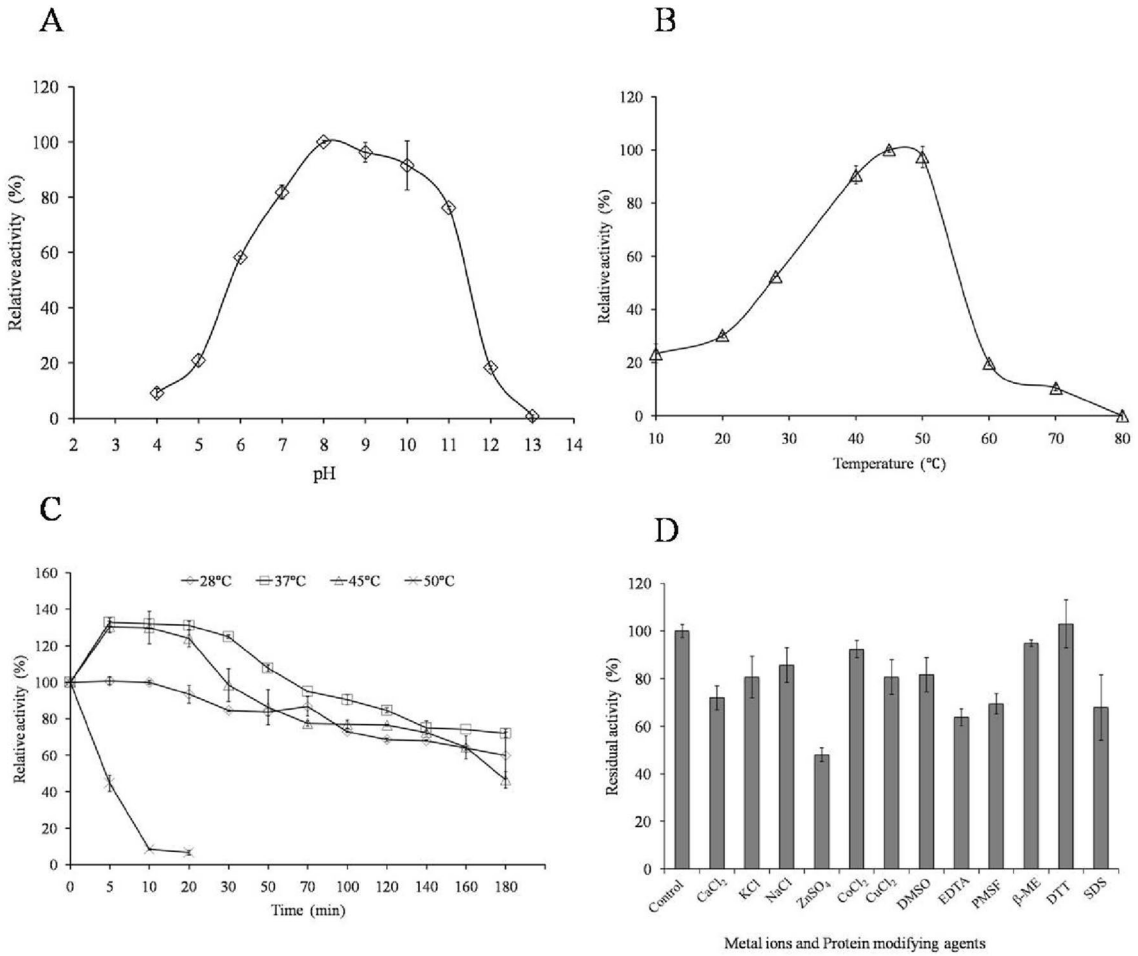

Fig. 2 Optimization of different reaction parameters for *Ps*44-ASNase II. **A** Effect of pH (3–13) on *Ps*44-ASNase II at 37 °C. **B** Effect of incubation temperature (10–80 °C) on *Ps*44-ASNase II at pH 8.5. **C** Thermostability profile of *Ps*44-ASNase II was studied by incubating at 28−50 °C for 200 min in Tris–HCl buffer (50.0 mM and 8.5 pH), and the residual *Ps*44-ASNase II activity was calculated. **D** Effect of metal ions and protein modifier agents on *Ps*44-ASNase II incubating at 37 °C for 60 min

Substrate specificity and kinetic parameters of *Ps*44-ASNase II

The Lineweaver–Burk plot was drawn to estimate the kinetic parameters by taking a different concentration of L-asparagine and L-glutamine (Fig. 3A). The K_m values of purified *Ps*44-ASNase II for L-asparagine and L-glutamine were found to be 0.559 ± 0.12 and 0.728 ± 0.086 mM, respectively. Similarly, V_{max} values of 29.41 ± 4.20 and 50.12 ± 3.54 U/mg for L-asparagine and L-glutamine were obtained, respectively (Table 2, Fig. 3B). The result shows that enzyme has more affinity for L-asparagine than L-glutamine. However, the turnover number (k_{cat}) for L-glutamine is more (30.91 ± 2.18 s^{-1}) than for L-asparagine (18.06 ± 2.59 s^{-1}) (Table 2). The K_m values of L-ASNase for *B. subtilis* B11-06 (Jia et al. 2013) and *Pectobacterium carotovorum* MTCC 1428 (Kumar et al. 2011) were 0.43 and 0.657 mM, respectively. The V_{max} of *Ps*44-ASNase II is considerably higher for L-glutamine than L-asparagine. In contrast, the K_m value is lower for L-ASNase, indicating that the enzyme acts on L-asparagine at lower concentrations than L-glutamine. Such a feature can be a favorable attribute where L-GLNase activity is not desired, like treating ALL. The high L-GLNase activity of L-ASNase has been reported as an undesirable feature for a therapeutic application. Therefore, the structural studies of *Ps*44-ASNase II were performed to know the possible molecular basis of a higher affinity for one substrate (L-asparagine) and a high turnover number for another (L-glutamine).

In-silico analysis of *Ps*44-ASNase II

BLASTp analysis of *Ps*44-ASNase II using the UniProtKB/Swiss-Prot database showed 95% similarity with L-ASNase of *P. putida* KT2440 (Q88K39.1). Further, the percent identity of *Ps*44-ASNase II was 85.64 with *Pseudomonas*

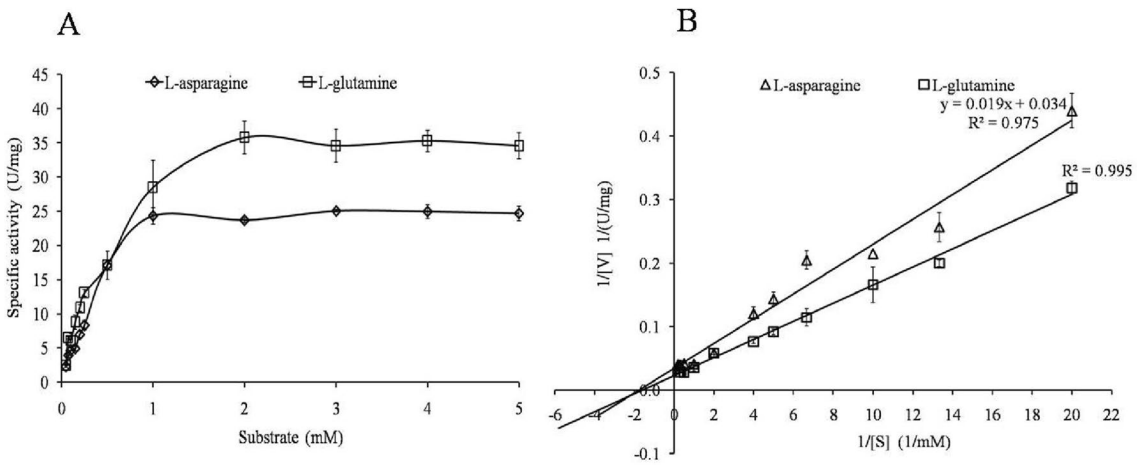

Fig. 3 Kinetic study of *Ps*44-ASNase II. **A** Effect of varying L-asparagine and L-glutamine concentration (0.25–5.0 mM) on *Ps*44-ASNase II activity. **B** Lineweaver–Burk plot for determining a kinetic parameter of *Ps*44-ASNase II for L-asparagine and L-glutamine

Table 2 Steady-state kinetic parameters for recombinant *Ps*44-ASNase II by using L-asparagine and L-glutamine (0.05–5.0 mM) and incubating the reaction at 37 °C for 15 min

	V_{max} (U/mg)	K_m (mM)	k_{cat} (s^{-1})	k_{cat}/K_m (s^{-1} mM^{-1})
L-Asparagine	29.41 ± 4.20	0.559 ± 0.12	18.06 ± 2.59	32.54 ± 2.42
L-Glutamine	50.12 ± 3.54	0.728 ± 0.086	30.91 ± 2.18	42.57 ± 2.07

fluorescens bv. A (*P. fluorescens*) (O68897.1), 61.89 with *Acinetobacter glutaminasificans* (*A. glutaminasificans*) (P10172.1), 48 with *E. coli* K-12 (P00805.2), and 47.26 with *E. chrysanthemi* (P06608.1) (Table S4). The *Ps*44-ASNase II showed two recognized structural domains, IlATGGTIA (residue 15–23) and GiVitHGTDTL (residue 94–104) when compared with selected L-ASNase sequences from most similarity index values (Fig. 4). The predicted active site for *Ps*44-ASNase II was Thr21 in the first domain and Thr101 in the second domain. The secondary structure analysis indicated random coil protein (40.83%), α-helices (34.91%), extended strands (19.82%), and β-turn (4.9%). Similarly, secondary structure analysis for L-ASNase of *P. putida* KT2440, *Pseudomonas* 7A, *E. coli*, and *E. chrysanthemi* has a similar trend as *Ps*44-ASNase II (Table S5).

Homology modeling of *Ps*44-ASNase II

BLASTp search in PDB database showed L-ASNase II of *Pseudomonas* sp. 7A (PDB ID: 3PGA) as the best template with 95.3% identity and 100% coverage. The crystal structure of L-ASNase from *Pseudomonas* sp. 7A was characterized by 2.0 Å resolution and studied for its catalytic residues and enzyme activity (Lubkowski et al. 1994). The crystal structure of L-ASNase of *Pseudomonas* sp. 7A was used as a template for homology modeling due to high sequence similarity, high query coverage, and phylogenetically closeness to *Ps*44-ASNase II. The modeled structure of *Ps*44-ASNase II was homotetrameric, and the topology of each chain was identical to the template (Fig. S6). The Ramachandran plot of the model showed 90.9% of amino acid residues in the most favored region, and 7.6% in the additional allowed region suggested for a good model (Fig. S7). Furthermore, verify3D score showed that 96.21 residues are arranged in secondary structure, and the ERRAT score was 96.68, which signifies the model's accuracy (Fig. S8). The overall structural analysis and validation suggest that the model structure of *Ps*44-ASNase II was suitable for further analysis.

Docking of L-asparagine and L-glutamine with *Ps*44-ASNase II and *Ec*-ASNase II provides a molecular basis for high L-GLNase activity in *Ps*44-ASNase II

The substrates L-asparagine and L-glutamine were docked with a homology model of *Ps*44-ASNase II and reference structure of L-ASNase (PDB ID: 1NNS) from *E. coli* (*Ec*-ASNase II) (Sanches et al. 2003). The catalytic role of threonine (Thr) for L-ASNase II activity is well studied using crystallography and mutational analysis (Kozak et al. 2000; Nomme et al. 2012; Brumano et al. 2019; Saeed et al.

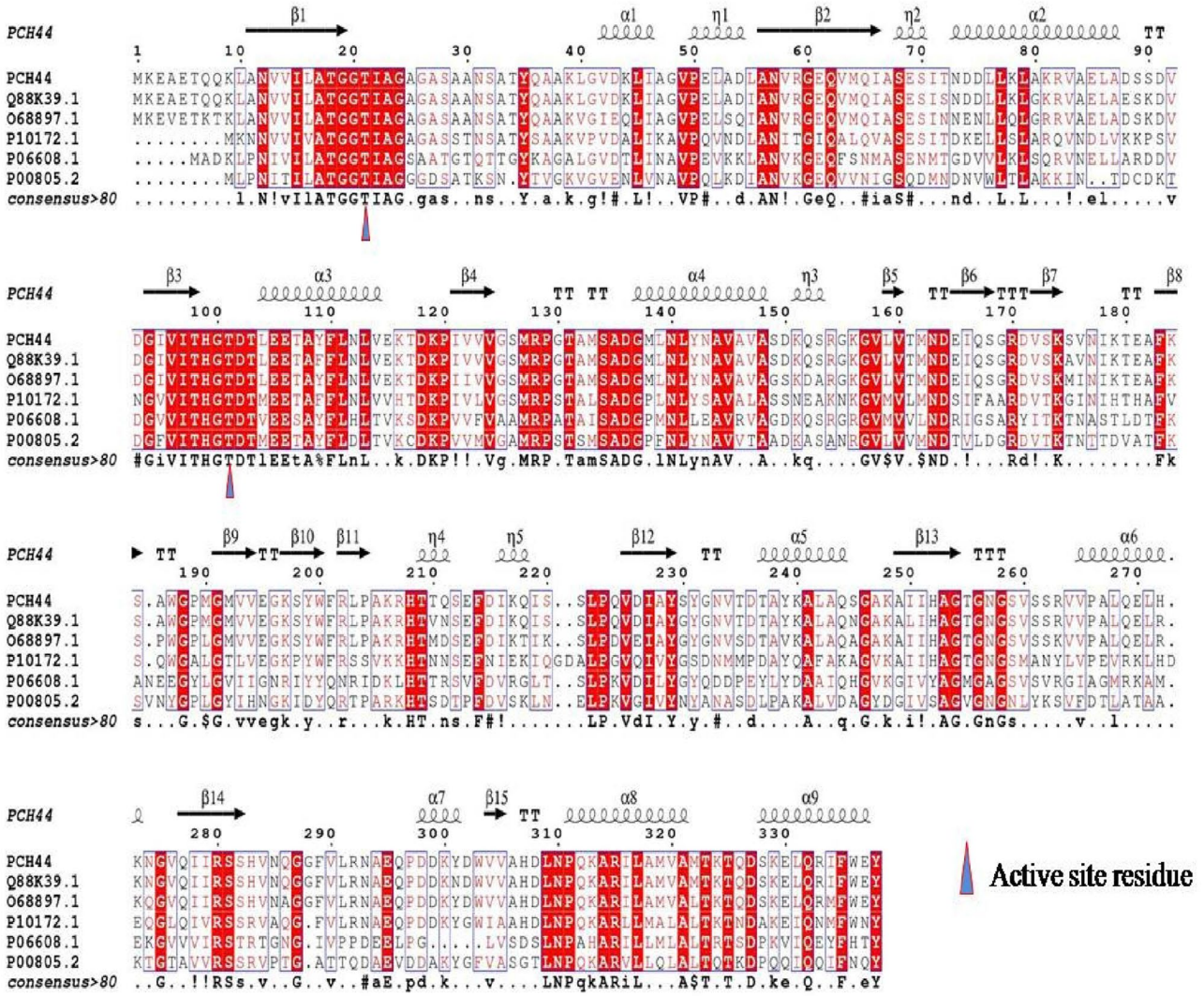

Fig. 4 Multiple sequence alignment of *Ps*44-ASNase II sequences using UniProt identifiers. Alignment of L-ASNase was performed by using ClustalW and ESPript 3.0. 'α' represents α-helix; 'β' represents β-sheet. The secondary structure was observed from the 3D structure (PDB ID: 3PGA) and reported at the top

2020). In short, L-ASNase mechanism of action involves the hydroxyl group of Thr, which initiates the nucleophilic attack on amine group of L-asparagine and forms an intermediate complex. It is followed by adding water molecules, resulting in aspartic acid and ammonium ions formation (Nguyen et al. 2016a, b; Lubkowski et al. 2020). Since the molecular structure of L-glutamine is similar to L-asparagine except for an additional methyl group, the mechanism of action is anticipated to be the same for both the substrates (Lubkowski et al. 2020)**.** Based on the literature and current findings, Thr12 and Thr89 in *Ec*-ASNase II and Thr21 and Thr101 in *Ps*44-ASNase II were selected for docking grid. The docking analysis of *Ps*44-ASNase II and *Ec*-ASNase II showed average binding energy of −3.11, −4.33 for L-glutamine and −2.59, −4.05 for L-asparagine, respectively. The binding energy of *Ec*-ASNase II for L-glutamine was lesser than *Ps*44-ASNase II, which showed a lower catalysis rate (Reddy et al. 2016; Lubkowski et al. 2020). Further, the distance from nucleophilic residue Thr101 and Thr21 to carbonyl NH_2 group of L-glutamine were 2.65 and 4.07 Å, whereas, for L-asparagine, the distance was observed at 2.95 and 3.62 Å, respectively (Fig. 5). The low binding energy of L-glutamine and closer proximity to catalytic Thr101 of *Ps*44-ASNase II correlate with kinetic data having a high turnover number for L-glutamine (30.91 s^{-1}) as compared to L-asparagine (18.06 s^{-1}).

The docked complexes of *Ps*44-ASNase II showed differences in the amino acids close (≤3.0 Å) with L-asparagine and L-glutamine ligands. For L-asparagine, the residues Thr101, Ser68, Glu69, and Asp102 are

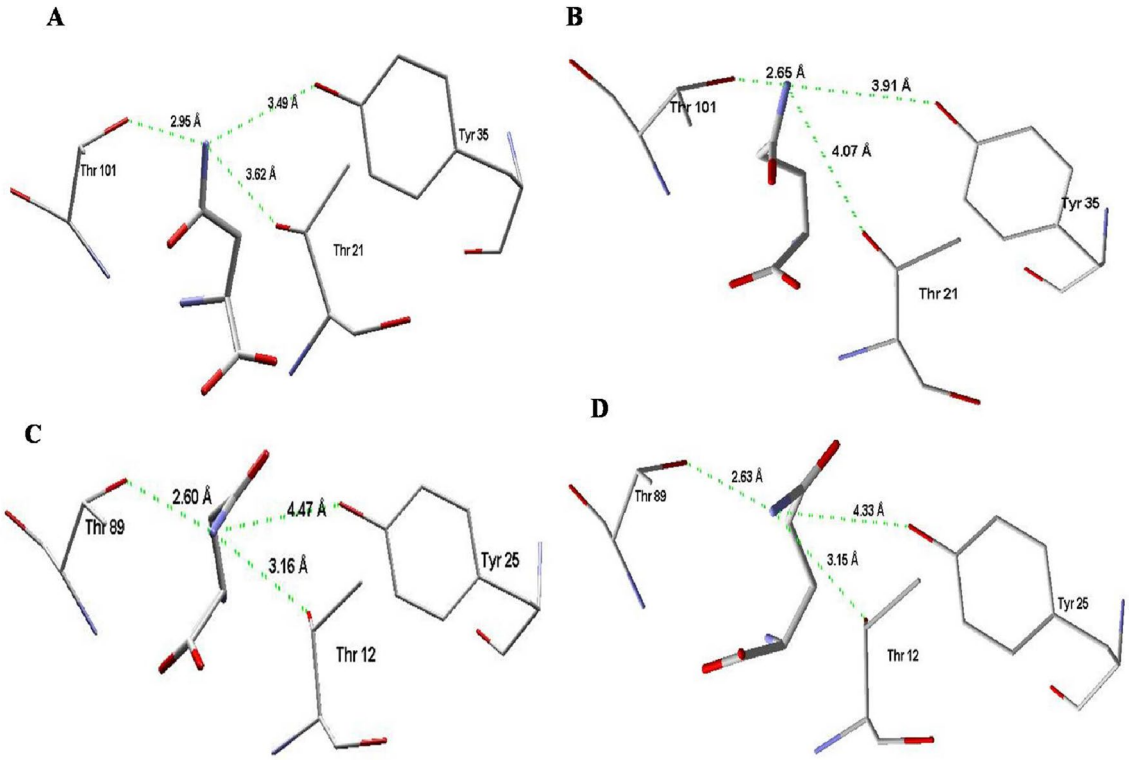

Fig. 5 Docking of L-ASNase II with L-asparagine and L-glutamine. **A**, **B** interaction of an amino group of L-asparagine and L-glutamine with the hydroxyl group of Thr21, Thr101 of *Ps*44-ASNase II. **C**, **D** Interaction of amino group of L-asparagine and L-glutamine with the hydroxyl group of Thr12, Thr89 of *Ec*-ASNase II. Distance between the NH_2 group of L-asparagine and L-glutamine with OH group of Thr21, Thr101 is 3.62, 2.95, and 4.07, 2.65, respectively, and in *Ec*-ASNase II Thr12 and Thr89 is 3.16, 2.60 and 3.15, 2.63 for L-asparagine and L-glutamine, respectively

within ≤ 3.0 Å, whereas Thr101, Thr21, Ser68, Glu69, and Asp102 are close to L-glutamine (Fig. 6A, B). The closeness of an additional nucleophile Thr21 to the carbonyl group of L-glutamine might be responsible for higher L-GLNase activity. In *Ec*-ASNase II, nucleophile Thr12 and Thr 89 are close to L-asparagine and L-glutamine. However, Thr12 is away from the carbonyl group of L-glutamine (Fig. 6C, D). The active sites of *Ps*44-ASNase II and *Ec*-ASNase II showed both conserved and diverged residues. The diverged residue within ≤3 Å of docked L-glutamine was Gln69 in *Ps*44-ASNase II and Ala114 for *Ec*-ASNase II. The variation of amino acids within 3.0 to 5.0 Å of the active site in *Ps*44-ASNase II and *Ec*-ASNase II were Ala37, Ala38, Ala67, Ser70, Ser126, and Glu 69 in place of Val, Gly, Gly, Asp, Ala, and Gln at the respective positions. These variations of amino acids might be responsible for higher L-GLNase activity of *Ps*44-ASNase II. Thus, comparing the docked complex of L-asparagine and L-glutamine provides a molecular basis for high L-GLNase activity in *Ps*44-ASNase II. The identified amino acid residues can be targeted in future studies for enzyme improvement through mutagenesis.

Conclusions

In the present study, the L-ASNase producing *Pseudomonas* sp. PCH44 was isolated from a high-altitude niche. The whole-genome sequencing and analysis of *Pseudomonas* sp. PCH44 revealed two L-*asn* genes belonging to Type I and II, where L-*asn* II is produced extracellularly. The *Ps*44-*asn* II gene was successfully cloned and expressed in a bacterial host *E. coli*. The *Ps*44-ASNase II was purified, and a native molecular weight of 148.0 kDa size in homotetrameric conformation was estimated, which is consistent with other reported molecular weights in the literature. However, *Ps*44-ASNase II has unique activity features of a wide pH range, high thermal stability, and half-life. In addition, the enzyme activity was not influenced positively by the metal ions and protein modifying agents. The in-silico studies revealed structural similarity of *Ps*44-ASNase II with L-ASNase of *P. putida* KT2440, *Pseudomonas* sp. 7A, *E. coli*, and *E. chrysanthemi*. The experimental data have shown that *Ps*44-ASNase II has a higher affinity for L-asparagine unlike a higher

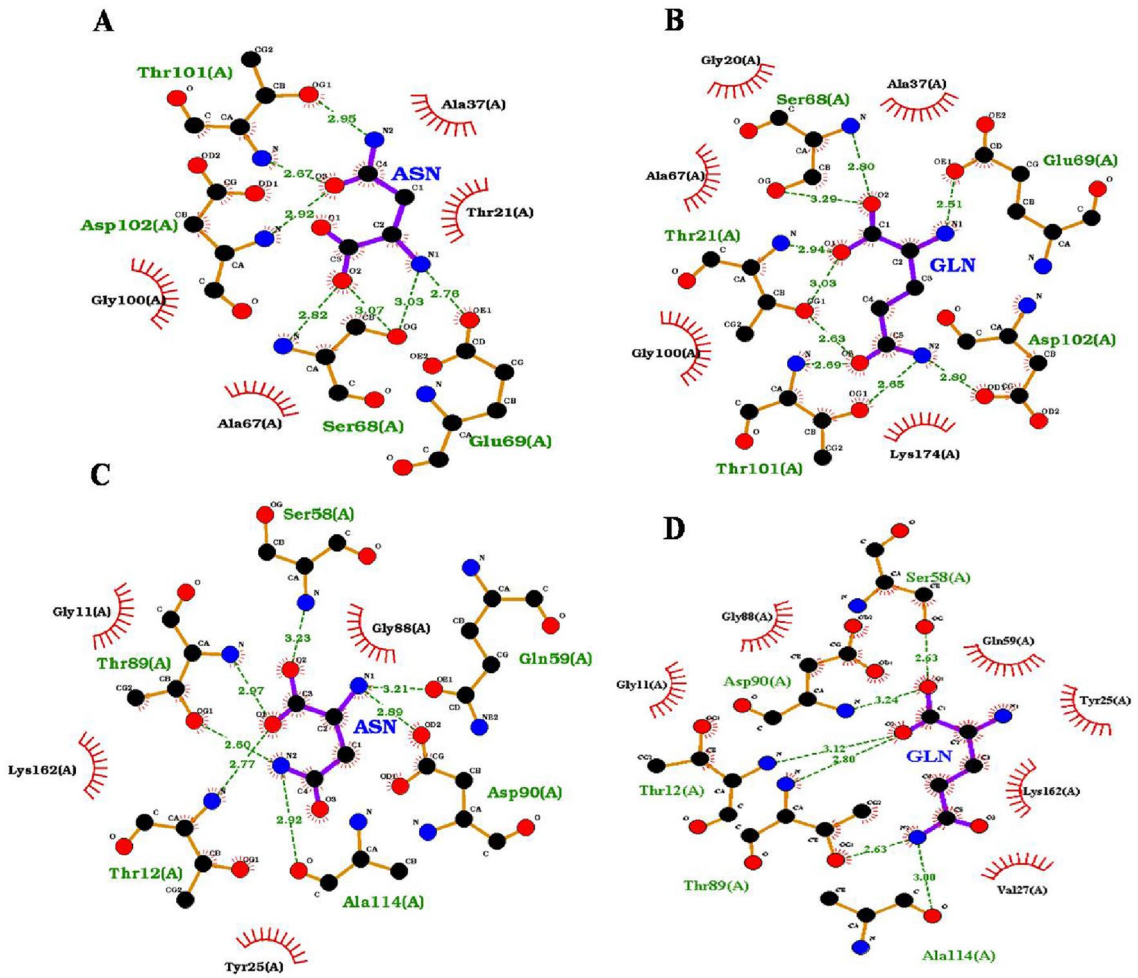

Fig. 6 LigPlot of interacting atoms of L-ASNase II. **A** *Ps*44-ASNase II with L-asparagine. **B** *Ps*44-ASNase II with L-glutamine. **C** *Ec*-ASNase II with L-asparagine. **D** *Ec*-ASNase II with L-glutamine

turnover number for L-glutamine. The contrasting observation was validated through the in-silico analysis of *Ps*44-ASNase II, where the possible amino acid residues were found for higher L-GLNase co-activity. In the future, critical amino acid residue of *Ps*44-ASNase II identified in present study can be targeted for mutagenesis to evaluate the enzyme for therapeutic applications.

Supplementary Information The online version contains supplementary material available at https://doi.org/10.1007/s13205-022-03224-0.

Acknowledgements Authors duly acknowledge Mr. Mohit Kumar Swarnkar for assistance in whole-genome sequencing.

Author contributions SK: Methodology, investigation, data curation, formal analysis, writing-original draft preparation. SD: Formal analysis, data curation. VP: Formal analysis, data curation. VrK: Formal analysis, data curation, writing. VK: Formal analysis, editing. SK: Resources. DS: Conceptualization, methodology, formal analysis, supervision, resources, visualization, writing-review and editing.

Funding Indian Council of Medical Research (ICMR), New Delhi is duly acknowledged for financial support in the form of Research Fellowship to SK & VP and Young Scientist award to Vr. K. SD duly acknowledges fellowship support from the Council of Scientific and Industrial Research (CSIR), New Delhi. VK also duly acknowledges DST, New Delhi, for the Young Scientist award. DS gratefully acknowledges financial support from CSIR, New Delhi, for researcht grants MLP0125 & 130.

Declarations

Conflict of interest The authors declare that they have no conflict of interest.

Research involving human participants and/or animals No human or animal participants were involved in this study.

Informed consent Informed consent rules were not applicable to this research because no human participants were involved.

References

Armenteros JA, Tsirigos KD, Sønderby CK et al (2019) SignalP 5.0 improves signal peptide predictions using deep neural networks. Nat Biotechnol 37:420–423. https://doi.org/10.1038/s41587-019-0036-z

Arnold K, Bordoli L, Kopp J, Schwede T (2006) The SWISS-MODEL workspace: A web-based environment for protein structure homology modelling. Bioinformatics 22:195–201. https://doi.org/10.1093/bioinformatics/bti770

Aziz RK, Bartels D, Best A et al (2008) The RAST Server: Rapid annotations using subsystems technology. BMC Genomics 9:1–15. https://doi.org/10.1186/1471-2164-9-75

Baskar G, Lalitha K, Aiswarya R, Naveenkumar R (2018) Synthesis, characterization and synergistic activity of cerium-selenium nanobiocomposite of fungal L-asparaginase against lung cancer. Mater Sci Eng C 93:809–815. https://doi.org/10.1016/j.msec.2018.08.051

Batool T, Makky EA, Jalal M, Yusoff MM (2016) A comprehensive review on L-asparaginase and its applications. Appl Biochem Biotechnol 178:900–923. https://doi.org/10.1007/s12010-015-1917-3

Bergmans HEN, Van Die IM, Hoekstra WPM (1981) Transformation in *Escherichia coli*: stages in the process. J Bacteriol 146:564–570. https://doi.org/10.1128/jb.146.2.564-570.1981

Bradford MM (1976) A rapid and sensitive method for the quantitation of microgram quantities of protein utilizing the principle of protein-dye binding. Anal Biochem 72:248–254

Brumano LP, da Silva FVS, Costa-Silva TA et al (2019) Development of L-asparaginase biobetters: Current research status and review of the desirable quality profiles. Front Bioeng Biotechnol 6:1–22. https://doi.org/10.3389/fbioe.2018.00212

Cooney DA, Capizzi RL, Handschumacher RE (1970) Evaluation of l-asparagine metabolism in animals and man. Cancer Res 30:929–935

Costa IM, Custódio Moura D, Meira Lima G et al (2022) Engineered asparaginase from *Erwinia chrysanthemi* enhances asparagine hydrolase activity and diminishes enzyme immunoreactivity-a new promise to treat acute lymphoblastic leukemia. J Chem Technol Biotechnol 97:228–239. https://doi.org/10.1002/jctb.6933

El-Naggar NEA, Deraz SF, El-Ewasy SM et al (2018) Purification, characterization and immunogenicity assessment of glutaminase free L-asparaginase from *Streptomyces brollosae* NEAE-115. BMC Pharmacol Toxicol 19:1–15. https://doi.org/10.1186/s40360-018-0242-1

Geourjon C, Deleage G (1995) Sopma: Significant improvements in protein secondary structure prediction by consensus prediction from multiple alignments. Bioinformatics 11:681–684. https://doi.org/10.1093/bioinformatics/11.6.681

Ghasemi A, Asad S, Kabiri M, Dabirmanesh B (2017) Cloning and characterization of *Halomonas elongata* L-asparaginase, a promising chemotherapeutic agent. Appl Microbiol Biotechnol 101:7227–7238. https://doi.org/10.1007/s00253-017-8456-5

Han S, Jung J, Park W (2014) Biochemical characterization of L-asparaginase in NaCl-tolerant *Staphylococcus* sp. OJ82 isolated from fermented seafood. J Microbiol Biotechnol 24:1096–1104

Hijiya N, Van Der Sluis IM (2016) Asparaginase-associated toxicity in children with acute lymphoblastic leukemia. Leuk Lymphoma 57:748–757. https://doi.org/10.3109/10428194.2015.1101098

Hill JM, Roberts J, Loeb E et al (1967) L-asparaginase therapy for leukemia and other malignant neoplasms: remission in human leukemia. JAMA 202:882–888

Huang L, Liu Y, Sun Y et al (2014) Biochemical characterization of a novel L-asparaginase with low glutaminase activity from *Rhizomucor miehei* and its application in food safety and leukemia treatment. Appl Environ Microbiol 80:1561–1569. https://doi.org/10.1128/AEM.03523-13

Imada A, Igarasi S, Nakahama K et al (1973) Asparaginase and glutaminase activities of micro-organisms. Microbiology 76:85–99

Jackson RC, Handschumacher RE (1970) *Escherichia coli* L-asparaginase. Catalytic activity and subunit nature. Biochemistry 9:3585–3590

Jia M, Xu M, He B, Rao Z (2013) Cloning, expression, and characterization of L-asparaginase from a newly isolated *Bacillus subtilis* B11–06. J Agric Food Chem 61:9428–9434. https://doi.org/10.1021/jf402636w

Kelo E, Noronkoski T, Mononen I (2009) Depletion of L-asparagine supply and apoptosis of leukemia cells induced by human glycosylasparaginase. Leukemia 23:1167–1171. https://doi.org/10.1038/leu.2008.387

Kidd JG (1953) Regression of transplanted lymphomas induced *in vivo* by means of normal guinea pig serum. J Exp Med 98:565–582. https://doi.org/10.1084/jem.98.6.565

Knott SRV, Wagenblast E, Khan S et al (2018) Asparagine bioavailability governs metastasis in a model of breast cancer. Nature 554:378–381. https://doi.org/10.1038/nature25465

Koren S, Walenz BP, Berlin K et al (2017) Canu: scalable and accurate long-read assembly via adaptive κ-mer weighting and repeat separation. Genome Res 27:722–736. https://doi.org/10.1101/gr.215087.116

Kornbrust BA, Stringer MA, Lange NEK et al (2009) Asparaginase–an enzyme for acrylamide reduction in food products. Enzyme Food Technol 2:59–87

Kozak M, Jaskólski M, Röhm KH (2000) Preliminary crystallographic studies of Y25F mutant of periplasmic *Escherichia coli* L-asparaginase. Acta Biochim Pol 47:807–814. https://doi.org/10.18388/abp.2000_3998

Kumar S, VenkataDasu V, Pakshirajan K (2011) Purification and characterization of glutaminase-free L-asparaginase from *Pectobacterium carotovorum* MTCC 1428. Bioresour Technol 102:2077–2082. https://doi.org/10.1016/j.biortech.2010.07.114

Kumar S, Stecher G, Li M et al (2018) MEGA X: Molecular evolutionary genetics analysis across computing platforms. Mol Biol Evol 35:1547–1549. https://doi.org/10.1093/molbev/msy096

Kumar V, Kumar S, Darnal S et al (2019) Optimized chromogenic dyes-based identification and quantitative evaluation of bacterial l-asparaginase with low/no glutaminase activity bioprospected from pristine niches in Indian trans-Himalaya. 3 Biotech 9:1–9. https://doi.org/10.1007/s13205-019-1810-9

Kumar V, Thakur V, Ambika et al (2020) Genomic insights revealed physiological diversity and industrial potential for *Glaciimonas* sp. PCH181 isolated from Satrundi glacier in Pangi-Chamba Himalaya. Genomics 112:637–646. https://doi.org/10.1016/j.ygeno.2019.04.016

Labrou NE, Muharram MM (2016) Biochemical characterization and immobilization of *Erwinia carotovora* L-asparaginase in a microplate for high-throughput biosensing of L-asparagine. Enzyme Microb Technol 92:86–93. https://doi.org/10.1016/j.enzmictec.2016.06.013

Laemmli UK (1970) Cleavage of structural proteins during the assembly of the head of bacteriophage T4. Nature 227:680–685

Laskowski RA, Swindells MB (2011) LigPlot+: multiple ligand–protein interaction diagrams for drug discovery. J Chem Inf Model 51:2778–2786. https://doi.org/10.1021/ci200227u

Lubkowski J, Wlodawer A, Ammon HL et al (1994) Structural characterization of *Pseudomonas* 7A glutaminase-asparaginase. Biochemistry 33:10257–10265

Lubkowski J, Vanegas J, Chan WK et al (2020) Mechanism of catalysis by l-Asparaginase. Biochemistry 59:1927–1945. https://doi.org/10.1021/acs.biochem.0c00116

Mahajan RV, Kumar V, Rajendran V et al (2014) Purification and characterization of a novel and robust L-asparaginase having low-glutaminase activity from *Bacillus licheniformis*: *In vitro* evaluation of anti-cancerous properties. PLoS ONE 9:11–16. https://doi.org/10.1371/journal.pone.0099037

Meghavarnam AK, Janakiraman S (2018) Evaluation of acrylamide reduction potential of L-asparaginase from *Fusarium culmorum* (ASP-87) in starchy products. LWT 89:32–37. https://doi.org/10.1016/j.lwt.2017.09.048

Narta UK, Kanwar SS, Azmi W (2007) Pharmacological and clinical evaluation of L-asparaginase in the treatment of leukemia. Crit Rev Oncol Hematol 61:208–221. https://doi.org/10.1016/j.critrevonc.2006.07.009

Nguyen HA, Su Y, Lavie A (2016a) Design and characterization of *Erwinia chrysanthemi* L-asparaginase variants with diminished L-glutaminase activity. J Biol Chem 291:17664–17676. https://doi.org/10.1074/jbc.M116.728485

Nguyen TTH, Nguyen CT, Le Nguyen TS et al (2016b) Optimization, purification, and characterization of recombinant L-asparaginase II in *Escherichia coli*. Afr J Biotechnol 15:1681–1691

Nomme J, Su Y, Konrad M et al (2012) Structures of apo and product-bound human L-asparaginase: insights into the mechanism of autoproteolysis and substrate hydrolysis. Biochemistry 51:6816–6826. https://doi.org/10.1021/bi300870g

Paul V, Tiwary BN (2020) An investigation on the acrylamide mitigation potential of L-asparaginase from *Aspergillus terreus* BV-C strain. Biocatal Agric Biotechnol 27:101677. https://doi.org/10.1016/j.bcab.2020.101677

Pokrovskaya MV, Aleksandrova SS, Pokrovsky VS et al (2012) Cloning, expression and characterization of the recombinant *Yersinia pseudotuberculosis* L-asparaginase. Protein Expr Purif 82:150–154. https://doi.org/10.1016/j.pep.2011.12.005

Pui CH, Campana D, Pei D et al (2009) Treating childhood acute lymphoblastic leukemia without cranial irradiation. N Engl J Med 360:2730–2741. https://doi.org/10.1056/nejmoa0900386

Radha R, Arumugam N, Gummadi SN (2018) Glutaminase free L-asparaginase from *Vibrio cholerae*: Heterologous expression, purification and biochemical characterization. Int J Biol Macromol 111:129–138. https://doi.org/10.1016/j.ijbiomac.2017.12.165

Reddy ER, Babu RS, Chandrasai PD, Madhuri P (2016) Exploration of the binding modes of L-asparaginase complexed with its amino acid substrates by molecular docking, dynamics and simulation. 3 Biotech 6:1–8. https://doi.org/10.1007/s13205-016-0422-x

Robert X, Gouet P (2014) Deciphering key features in protein structures with the new ENDscript server. Nucleic Acids Res 42:320–324. https://doi.org/10.1093/nar/gku316

Saeed H, Hemida A, El-Nikhely N et al (2020) Highly efficient *Pyrococcus furiosus* recombinant L-asparaginase with no glutaminase activity: Expression, purification, functional characterization, and cytotoxicity on THP-1, A549 and Caco-2 cell lines. Int J Biol Macromol 156:812–828. https://doi.org/10.1016/j.ijbiomac.2020.04.080

Safary A, Moniri R, Hamzeh-Mivehroud M, Dastmalchi S (2019) Highly efficient novel recombinant L-asparaginase with no glutaminase activity from a new halo-thermotolerant *Bacillus* strain. BioImpacts 9:15–23. https://doi.org/10.15171/bi.2019.03

Sanches M, Alexandre J, Barbosa RG et al (2003) Biological crystallography structural comparison of *Escherichia coli* L-asparaginase in two monoclinic space groups. Acta Cryst 59:416–422. https://doi.org/10.1107/S0907444902021200

Schalk AM, Nguyen HA, Rigouin C, Lavie A (2014) Identification and structural analysis of an L-asparaginase enzyme from guinea pig with putative tumor cell killing properties. J Biol Chem 289:33175–33186. https://doi.org/10.1074/jbc.M114.609552

Shi R, Liu Y, Mu Q et al (2017) Biochemical characterization of a novel L-asparaginase from *Paenibacillus barengoltzii* being suitable for acrylamide reduction in potato chips and mooncakes. Int J Biol Macromol 96:93–99. https://doi.org/10.1016/j.ijbiomac.2016.11.115

Silverman LB, Gelber RD, Dalton VK et al (2001) Improved outcome for children with acute lymphoblastic leukemia: Results of Dana-Farber Consortium Protocol 91–01. Blood 97:1211–1218. https://doi.org/10.1182/blood.V97.5.1211

Singh Y, Gundampati RK, Jagannadham MV, Srivastava SK (2013) Extracellular L-asparaginase from a protease-deficient *Bacillus aryabhattai* ITBHU02: Purification, biochemical characterization, and evaluation of antineoplastic activity in vitro. Appl Biochem Biotechnol 171:1759–1774. https://doi.org/10.1007/s12010-013-0455-0

Sokolov NN (1976) Sulfhydryl groups of L-asparaginase A from *Pseudomonas fluorescens* AG. Biokhimiia (moscow, Russia) 41:727–731

Soncini D, Minetto P, Martinuzzi C et al (2020) Amino acid depletion triggered by L-asparaginase sensitizes MM cells to carfilzomib by inducing mitochondria ROS-mediated cell death. Blood Adv 4:4312–4326. https://doi.org/10.1182/BLOODADVANCES.2020001639

Tatusova T, Dicuccio M, Badretdin A et al (2016) NCBI prokaryotic genome annotation pipeline. Nucleic Acids Res 44:6614–6624. https://doi.org/10.1093/nar/gkw569

Thakur V, Kumar V, Kumar S et al (2018) Diverse culturable bacterial communities with cellulolytic potential revealed from pristine habitat in Indian trans-Himalaya. Can J Microbiol 64:798–808. https://doi.org/10.1139/cjm-2017-0754

Trott O, Olson AJ (2010) AutoDockVina: improving the speed and accuracy of docking with a new scoring function, efficient optimization, and multithreading. J Comput Chem 31:455–461

Tundisi LL, Coêlho DF, Zanchetta B et al (2017) L-Asparaginase purification. Sep Purif Rev 46:35–43. https://doi.org/10.1080/15422119.2016.1184167

Verma N, Kumar K, Kaur G, Anand S (2007) L-asparaginase: A promising chemotherapeutic agent. Crit Rev Biotechnol 27:45–62. https://doi.org/10.1080/07388550601173926

Vimal A, Kumar A (2017) Biotechnological production and practical application of L-asparaginase enzyme. Biotechnol Genet Eng Rev 33:40–61. https://doi.org/10.1080/02648725.2017.1357294

Wang H, Li D, Li JT et al (2009) Side effects of L-asparaginase during therapies for remission induction and maintenance in children with acute lymphocytic leukemia. J Exp Hematol 17:739–741

Warangkar SC, Khobragade CN (2010) Purification, characterization, and effect of thiol compounds on activity of the *Erwinia carotovora* L-asparaginase. Enzyme Res 2010:2010. https://doi.org/10.4061/2010/165878

Wingfield PT (2015) Overview of the purification of recombinant proteins. Curr Protoc Protein Sci 80:6–11. https://doi.org/10.1002/0471140864.ps0601s80

Yun MK, Nourse A, White SW et al (2007) Crystal structure and allosteric regulation of the cytoplasmic *Escherichia coli* L-asparaginase I. J Mol Biol 369:794–811. https://doi.org/10.1016/j.jmb.2007.03.061